

An Analysis of Intersecting Adiabatic Flows using the Semi-Lagrangian Galerkin Method

R. Omata
Department of Civil Engineering
Chuo University, Tokyo, Japan

Abstract

The purpose of this study is to express the change of flow pattern in the intersecting adiabatic flow using the difference of the flow channel and of the degrees using the Semi-Lagrangian Galerkin finite element method. The conservation of mass and momentum are used as the basic equation. To calculate the governing equations, the Semi-Lagrangian method is applied as an analytical technique. A characteristic of this method is based on the fact that the governing equations can be divided into two phases which are advection and non-advection at an instantaneous time of calculation. As the temporal discretization, the advection phase is calculated using the characteristic method, and the non-advection phase is calculated using the implicit method. In the spatial discretization the Galerkin method is adopted. To perform high accurate computation, we use the third-order Hermitian type element. This element has ten degrees of freedom, which consist of function values of nodes of the triangle and first order derivatives on each nodes and a function value of centre of the triangle.

Keywords: semi-Lagrangian Galerkin method, conservation of mass, conservation of momentum, characteristic method, implicit scheme, Hermitian type element.

1 Introduction

An incompressible viscous fluid is mostly used assumption in the field of computational fluid dynamics in recent years. However, actually, only a few phenomena which can be assumed as the incompressible in natural phenomena. In fact, it is necessary to consider compressibility if we deal with much broader phenomena. In order to consider the compressibility, it is mainstream to use the full compressible equations including energy conservation equation. However, since a lot of variables should be treated and formulation is complicated, heavy computational load is necessary to solve

the full compressible equation system.

In this study, we derived the equation system in which density is considered as a variable assuming adiabatic state. In order to obtain the pressure, the Poisson's law which is an expression of relation of pressure and density is applied for the equation of state. The governing equation is assumed to consist of both advection and non-advection terms. In case of the calculation equation of advection term, sometimes, instability of the computation occurs. Thus, the characteristic method which is useful for the calculation of advection term is applied. Unknown function at the upstream side on a characteristic curve is approximated by the Hermitian type element in this study. Also in calculation of non-advection terms, we apply the same-order interpolation for velocity and density on the same element. We call this method as the Semi-Lagrangian Galerkin method. The Hermitian type element has 10-degrees of freedom which consist of function values of node of the triangle and first order derivatives on each node and a function value of center of gravity. The present interpolation is used in high precision fluid flow analysis of the intersecting flow.

2 Basic Equation

In this study, the inditial notation and the summation convention are used to express equation. The governing equations can be expressed using velocity u_i and density ρ as follows: the conservation of mass

$$\frac{D\rho}{Dt} + \rho u_{i,i} = 0 \quad \text{in } \Omega \quad (1)$$

and the conservation of momentum

$$\rho \frac{Du_i}{Dt} - \tau_{ij,j} = 0 \quad \text{in } \Omega \quad (2)$$

where τ_{ij} means the total stress

$$\tau_{ij} = -p\delta_{ij} + \lambda\delta_{ij}u_{k,k} + \mu(u_{i,j} + u_{j,i}) \quad (3)$$

where δ_{ij} is the Kronecker delta, and λ and μ are viscosity coefficients. Assuming the adiabatic flow, the equation of state can be expressed as follows:

$$\left(\frac{p}{p_0}\right) = \left(\frac{\rho}{\rho_0}\right)^\gamma \quad \text{in } \Omega \quad (4)$$

where p is the pressure and γ is the gass constant. The reference values of pressure and density are denoted by p_0 and ρ_0 . The viscosity coefficients λ can be expressed as:

$$\lambda = -\frac{2}{3}\mu \quad (5)$$

The material derivative is denoted by

$$\frac{D}{Dt} = \frac{\partial}{\partial t} + u_i \frac{\partial}{\partial x_i} \quad (6)$$

3 Characteristic Method

Let the position of a virtual fluid particle in time φ which is in a position x at time t be $X(x, t; \varphi)$, trajectory of a particle is expressed by the following ordinary differential equation.

$$\frac{dX_i}{d\varphi} = u_i(X_i(x_i, t; \varphi), \varphi), \quad (7)$$

$$X_i(x_i, t; t) = x_i \quad (8)$$

Let n denote time step, and the time increment be Δt . The time differentiation term in equations (1) and (2) can be approximated as follows.

$$\frac{Du_i}{Dt} \doteq \frac{u_i^{n+1}(x) - \tilde{u}_i(x)}{\Delta t} \quad (9)$$

Here, \tilde{u}_i is the velocity at the position of the upstream point $X(x)$. In this study, to find upstream point, the predictor-corrector method is applied.

$$X_{i1}^n(x) = x_i - u_i^n(x)\Delta t \quad (10)$$

$$X_{i2}^n(x) = x_i - \frac{\Delta t}{2}(u_i^n(X_{i1}^n(x)) + u_i^{n+1}(x)) \quad (11)$$

where $X_2^n(x)$ is the upstream point, and $\tilde{u}(x)$ is calculated by the following advection calculation.

$$\tilde{u}_i = u_i(X_{i2}^n(x)) \quad (12)$$

$$\tilde{u}_e = u_i(X_e^n(x)) \quad (13)$$

$$\frac{\partial \tilde{u}_i}{\partial x_j} = (\delta_{jk} - \Delta t \frac{\partial u_k^{n+1}}{\partial x_j}) \frac{\partial u_i^n(X_{i2}^n)}{\partial x_k} \quad (14)$$

The implicit scheme is applied to the calculation method of the non-advection term.

3.1 Finite Element Equation

The discretized equation in time is expressed as follows,

$$\bar{\rho} \frac{u_i^{n+1} - \tilde{u}_i}{\Delta t} + \bar{\kappa} \rho_{,i}^{n+1} - \lambda \delta_{ij} u_{k,kj}^{n+1} - \mu (u_{i,j}^{n+1} + u_{j,i}^{n+1})_{,j} = 0 \quad \text{in } \Omega \quad (15)$$

$$\frac{\rho^{n+1} - \tilde{\rho}}{\Delta t} + \bar{\rho} u_{i,i}^{n+1} = 0 \quad \text{in } \Omega \quad (16)$$

where $\bar{\rho}$ and $\bar{\kappa}$ are as follows.

$$\bar{\rho} = \rho^n \quad \bar{\kappa} = \frac{\gamma p_0}{\bar{\rho}} \left(\frac{\bar{\rho}}{\rho_0} \right)^\gamma,$$

In equations (15) and (16), equations (9) is used.

4 Finite Element Interpolation

4.1 Interpolation Function

As an interpolation, the Hermitian type element as shown in Figure 1 is applied. The

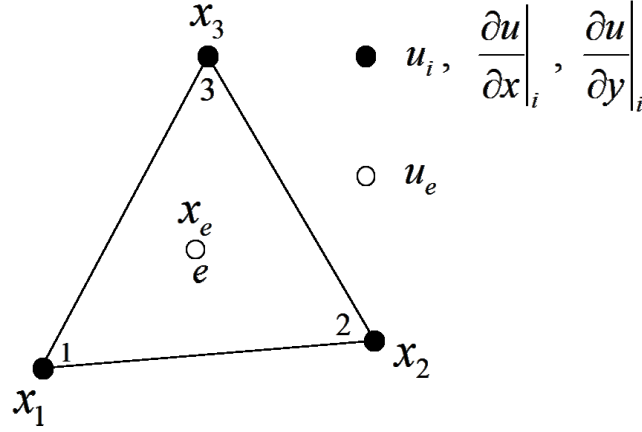


Figure 1: Hermitian type element

Hermitian type element has 10 degrees of freedom which consist of function values and first order derivatives on each node and a function value on the center of gravity. The finite element approximation can be expressed as:

$$u_i = \sum_{j=1}^3 (H_{0j}u_j + H_{xj} \frac{\partial u_j}{\partial x} + H_{yj} \frac{\partial u_j}{\partial y}) + H_{0e}u_e \quad (17)$$

where H_{0i} , H_{xi} , H_{yi} , and H_{0e} are interpolation functions, which are shown by the area coordinate L_i as:

$$\begin{cases} H_{0i} = L_i^2(3 - 2L_i) - 7L_1L_2L_3 \\ H_{xi} = L_i^2(x_{ji}L_j - x_{ik}L_k) - (x_{ji} - x_{ik})L_1L_2L_3 \\ H_{yi} = L_i^2(y_{ji}L_j - y_{ik}L_k) - (y_{ji} - y_{ik})L_1L_2L_3 \\ H_{0e} = 27L_1L_2L_3 \end{cases} \quad (18)$$

$$x_{ij} = x_i - x_j, y_{ij} = y_i - y_j \quad (19)$$

where (x_i, y_i) means coordinates at nodal point i , and (i, j, k) is even permutation of $(1, 2, 3)$. The interpolation of the first derivative by x is expressed as;

$$\frac{\partial u_i}{\partial x} = \sum_{j=1}^3 \left(\frac{\partial H_{0j}}{\partial x} u_j + \frac{\partial H_{xj}}{\partial x} \frac{\partial u_j}{\partial x} + \frac{\partial H_{yj}}{\partial x} \frac{\partial u_j}{\partial y} \right) + \frac{\partial H_{0e}}{\partial x} u_e \quad (20)$$

Each component of the first derivative by x can be expressed as follows.

$$\left\{ \begin{array}{l} \frac{\partial H_{0i}}{\partial x} = 2b_i L_i (3 - 2L_i) - 7(b_1 L_2 L_3 + L_1 b_2 L_3 + L_1 L_2 b_3) - 2b_i L_i^2 \\ \frac{\partial H_{xi}}{\partial x} = 2b_i L_i (c_k L_j - c_j L_k) - b_1 (c_k - c_j) L_2 L_3 - b_2 (c_k - c_j) L_1 L_3 - b_3 (c_k - c_j) L_1 L_2 + (b_j c_k - b_k c_j) L_i \\ \frac{\partial H_{yi}}{\partial x} = 2b_i L_i (b_j L_k - b_k L_j) - b_1 (b_j - b_k) L_2 L_3 - b_2 (b_j - b_k) L_1 L_3 - b_3 (b_j - b_k) L_1 L_2 \\ \frac{\partial H_{0e}}{\partial x} = 27(b_1 L_2 L_3 + L_1 b_2 L_3 + L_1 L_2 b_3) \end{array} \right.$$

In the same manner, each component of the first derivative by y can be obtained as follows.

$$\left\{ \begin{array}{l} \frac{\partial H_{0i}}{\partial y} = 2c_i L_i (3 - 2L_i) - 7(c_1 L_2 L_3 + L_1 c_2 L_3 + L_1 L_2 c_3) - 2c_i L_i^2 \\ \frac{\partial H_{xi}}{\partial y} = 2c_i L_i (c_k L_j - c_j L_k) - c_1 (c_k - c_j) L_2 L_3 - c_2 (c_k - c_j) L_1 L_3 - c_3 (c_k - c_j) L_1 L_2 \\ \frac{\partial H_{yi}}{\partial y} = 2c_i L_i (b_j L_k - b_k L_j) - c_1 (b_j - b_k) L_2 L_3 - c_2 (b_j - b_k) L_1 L_3 - c_3 (b_j - b_k) L_1 L_2 + (b_j c_k - b_k c_j) L_i \\ \frac{\partial H_{0e}}{\partial y} = 27(c_1 L_2 L_3 + L_1 c_2 L_3 + L_1 L_2 c_3) \end{array} \right.$$

In equations (21) and (22), b_i and c_i are;

$$b_i = \frac{1}{2A} (y_j - y_k) \quad (23)$$

$$c_i = \frac{1}{2A} (x_k - x_j) \quad (24)$$

where, A is the area of an element.

5 Finite Element Equation

The finite element equations of the governing equation are expressed as:

$$M_{\alpha\beta} \frac{u_{\beta i}^{n+1} - \tilde{u}_{\beta i}}{\Delta t} - G_{\alpha i\beta} \rho_{\beta}^{n+1} + S_{\alpha i\beta j} u_{\beta j}^{n+1} = F_{\alpha i} \quad in \Omega \quad (25)$$

$$N_{\alpha\beta} \frac{\rho_{\beta}^{n+1} - \tilde{\rho}_{\beta}}{\Delta t} + B_{\alpha\beta i} u_{\beta i}^{n+1} = 0 \quad in \Omega \quad (26)$$

Coefficient matrixes are as;

$$M_{\alpha\beta} = \bar{\rho} \int_{\Omega_e} H_{\alpha} H_{\beta} d\Omega, \quad G_{\alpha i\beta} = \bar{\kappa} \int_{\Omega_e} H_{\alpha, i} H_{\beta} d\Omega,$$

$$S_{\alpha i\beta j} = \lambda \int_{\Omega_e} H_{\alpha, i} H_{\beta, j} d\Omega + \mu \int_{\Omega_e} H_{\alpha, k} H_{\beta, k} \delta_{ij} d\Omega + \mu \int_{\Omega_e} H_{\alpha, j} H_{\beta, i} d\Omega,$$

$$N_{\alpha\beta} = \int_{\Omega_e} H_{\alpha} H_{\beta} d\Omega, \quad B_{\alpha\beta i} = \bar{\rho} \int_{\Omega_e} H_{\alpha} H_{\beta, i} d\Omega, \quad F_{\alpha i} = \int_{\Gamma} H_{\alpha} t_i d\Gamma$$

6 Numerical Study

As a numerical study, an intersecting flow is analyzed in three cases using the Semi-Lagrangian Galerkin Method. In case1 and 2 are the same computational domain. The Reynolds number is set to $Re = 6000$. Case3 is analyzed the complicated domain. The Reynolds number is set to $Re = 9000$. The intersecting flow is analyzed assuming the adiabatic flow. In case1 and 2, we compare the difference of flow pattern by the symmetric and asymmetric inflows.

6.1 Case1

Computational domain and boundary conditions are expressed in Figure 3. Each values given as boundary conditions are expressed as follows. Up and down inflow boundaries are given symmetric inflow, and the velocity of face of walls are given zero. The finite element mesh is shown in Figures 4 to 6. Each crossing angles are 30 and 60 and 90 degrees, respectively. In Figure 4, total numbers of nodes and elements are 5145 and 9532, respectively. In Figure 5, total numbers of nodes and elements are 5061 and 9328, respectively. In Figure 6, total numbers of nodes and elements are 5303 and 9804, respectively. The shapes of channel are treated pipelines in case 1 and 2.

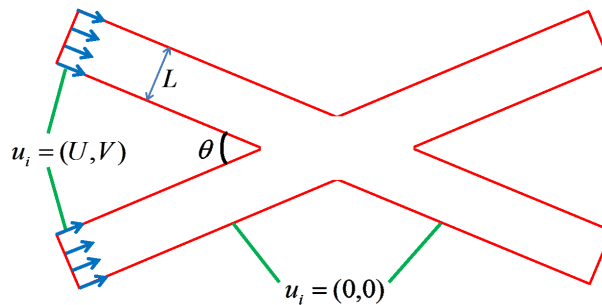


Figure 3: Computational domain

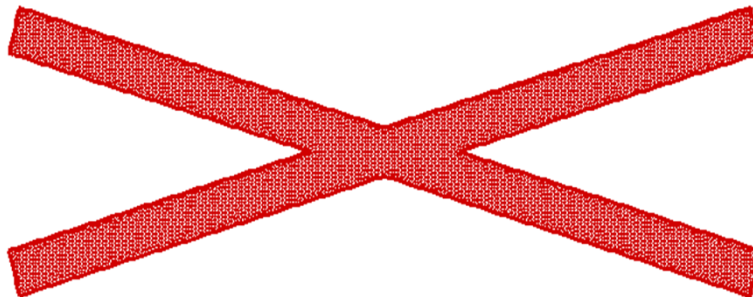


Figure 4: Finite element mesh of 30 degree

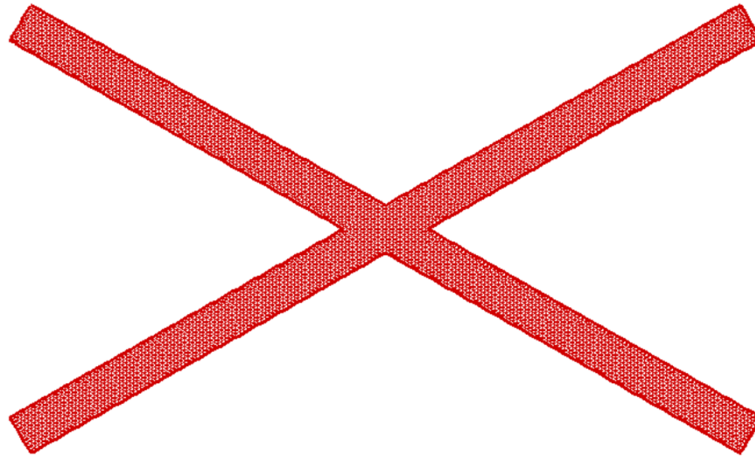


Figure 5: Finite element mesh of 60 degree

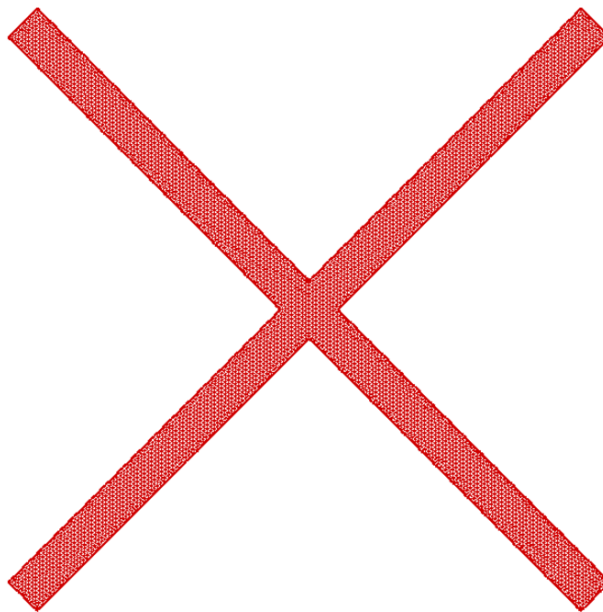


Figure 6: Finite element mesh of 90 degree

6.2 Case2

Computational domain and boundary conditions are expressed in Figure 7. Each values given as boundary conditions are expressed as follows. Up and down inflow boundaries are given asymmetric inflow of 1:1.2, and the velocity of face of walls are given zero. The crossing angles and the finite element mesh are same as case1. We compare the difference of form of vortex and the asymmetry of flows.

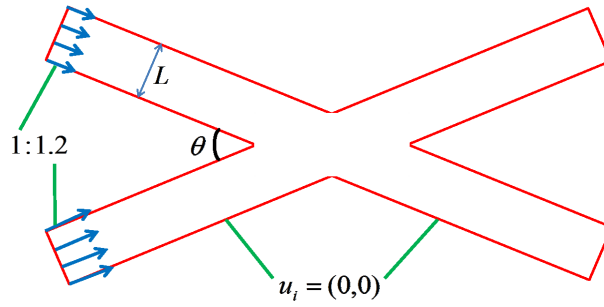


Figure 7: Computational domain

6.3 Case3

Computational domain and boundary conditions are expressed in Figure 8. As boundary conditions, Γ_U , the velocity in same direction along the rhombus lines. On Γ_S , periodic boundary is assumed. On Γ_B , the condition that the tangential velocity around a body is zero is applied. The finite element mesh is shown in Figure 9. Total numbers of nodes and elements are 13104 and 24976, respectively. The total number of nodes around the body is 32. The shape of bodies sets the rhombus with smooth edge.

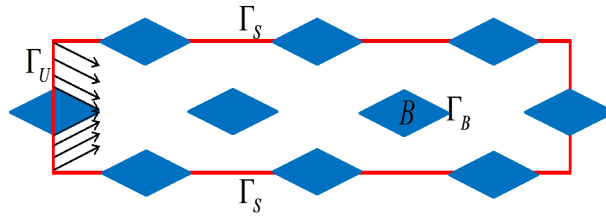


Figure 8: Computational domain



Figure 9: Finite element mesh

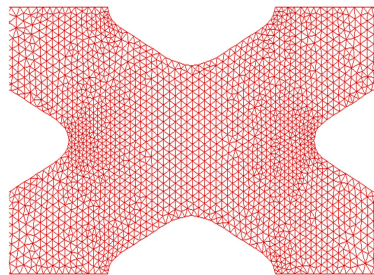


Figure 10: Finite element mesh around bodies

7 Numerical Results

7.1 Case1

As the numerical results, Figures 11 to 16 show stream lines in the flow in pipelines. The streamlines comes off and adheres to pipelines. In Figures 11 and 12, the vortices occur symmetry and disappear at end. The more expand the crossing angle, the more not to disappear the vortices. Please look at Figure 15 and 16. We can't confirm but the vortices occur both Figures 15 and 16. One of the causes of this is centrifugal force. The more expand the crossing angle, the more this affects.

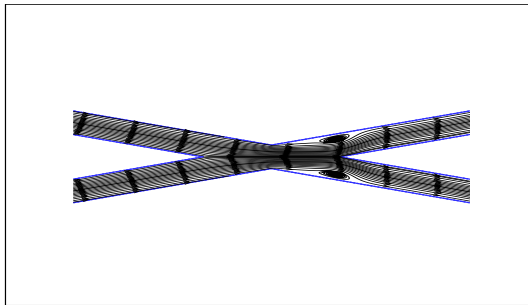


Figure 11: Stream lines of degree of 30

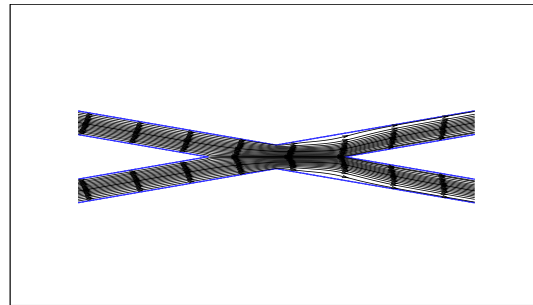


Figure 12: Stream lines of degree of 30

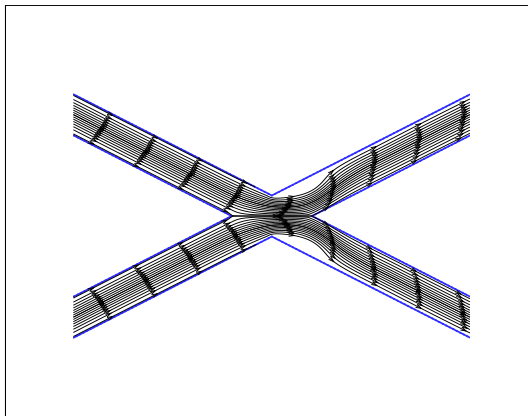


Figure 13: Stream lines of degree of 60

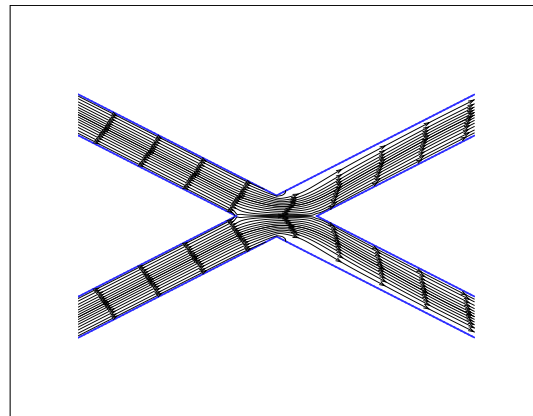


Figure 14: Stream lines of degree of 60

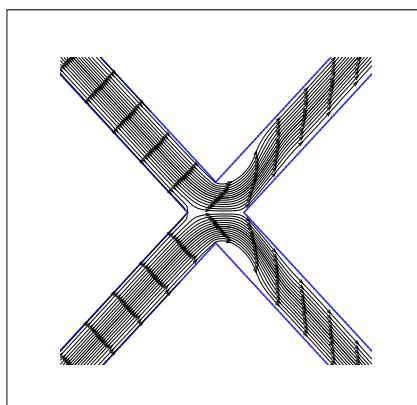


Figure 15: Stream lines of degree of 90

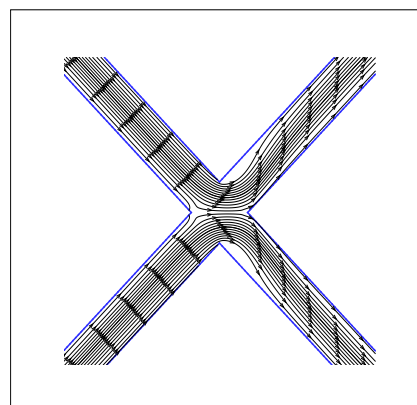


Figure 16: Stream lines of degree of 90

7.2 Case2

In Figures 17 to 22 show stream lines in the flow in pipelines. All figures show the asymmetric flows. The streamlines comes off and adheres to pipelines. In Figures 17 and 18, the vortices occur asymmetry and disappear at end. In Figures 19 and 20, the vortices occur asymmetry but not to disappear and exist asymmetry. The biggest reason of this is the asymmetric inflows.

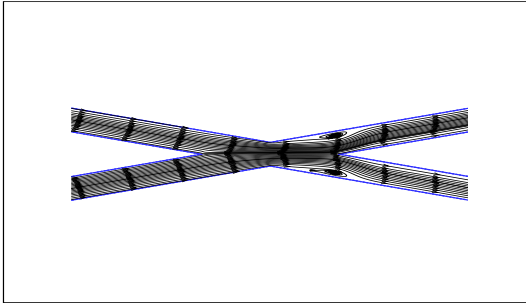


Figure 17: Stream lines of degree of 30

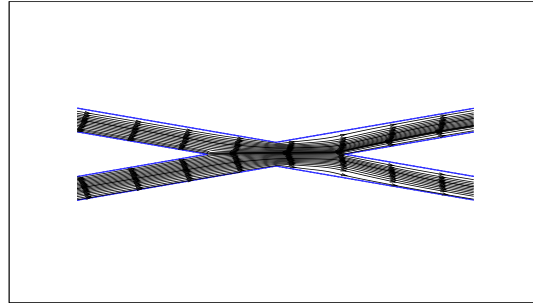


Figure 18: Stream lines of degree of 30

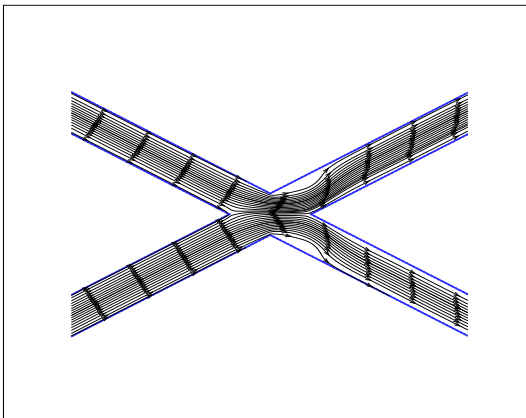


Figure 19: Stream lines of degree of 60

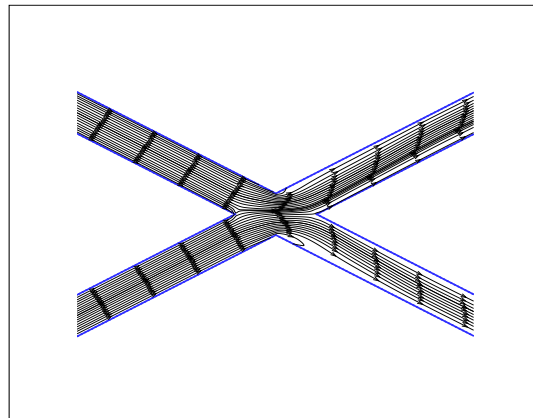


Figure 20: Stream lines of degree of 60

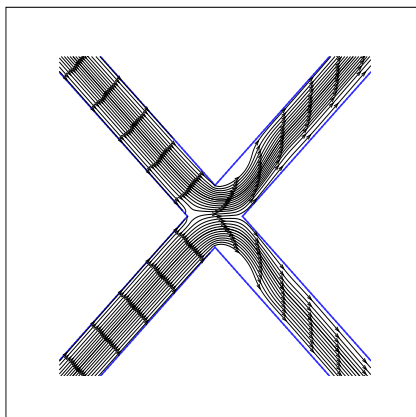


Figure 21: Stream lines of degree of 90

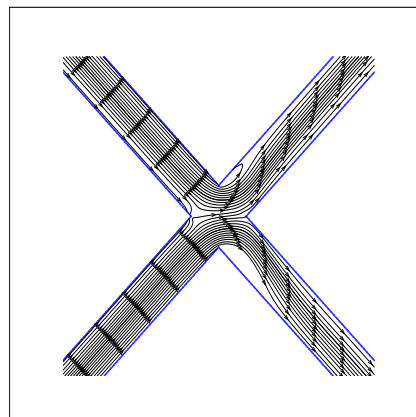


Figure 22: Stream lines of degree of 90

7.3 Case3

In Figures 23 to 25 are velocity distribution in the deformed X-channel and expanded figure of the velocity. In Figure 25, the stream line is shown. In this case, in spite of the symmetric inflow is given but the velocity is shown asymmetry. The biggest reason of this is given the periodic boundary. Therefore, there are no restriction in up and down boundaries.

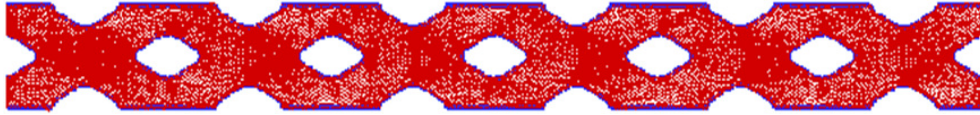


Figure 23: Velocity distribution of deformed X-channel

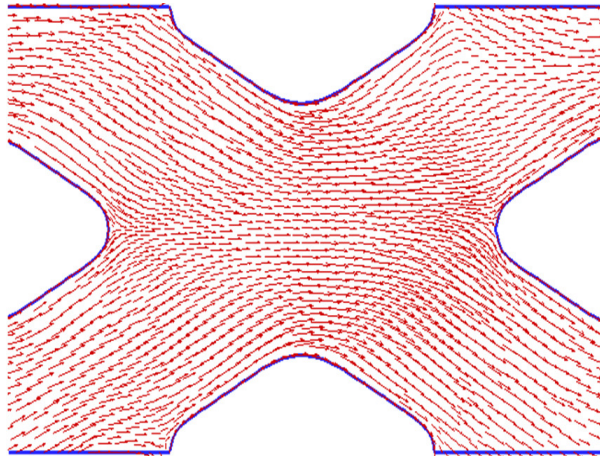


Figure 24: Velocity distribution of near deformed X-channel



Figure 25: Stream lines of deformed X-channel

8 Conclusion

In this paper, the intersecting flow is analyzed using the Semi-Lagrange Galerkin method. The flows in different crossing angles are confirmed. We can confirm the symmetric and asymmetric flow patterns that depend on the differences in the boundary conditions and the finite element mesh.

References

- [1] M. Utamura, H. Kimura, R. Kajita, “Generalized Hydraulic Diameter for The Development of High Performance Microchannel Heat Exchangers”.

- [2] N. Tsuzuki, Y. Kato, Y. Muto, T. Ishizuka, M. Utamura, M. Aritomi, “Nusselt Number Correlation of Microchannel Heat Exchanger with S-Shaped Fins”.
- [3] S. Umeda, Wen-Jei YANG, “Characteristics of Flow in the Intersecting Region of Converging/Diverging Flow Pairs”.